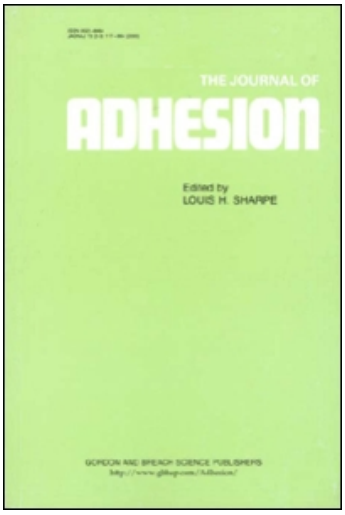

The Journal of Adhesion
Publication details, including instructions for authors and subscription information:
http://www.informaworld.com/smpp/title~content=t713453635

Viscoelastic and Processing Effects on the Fiber-Matrix Interphase Strength. Part I. The Effects of Loading Rate, Test Temperature, Fiber Sizing and Global Strain Level

Erol Sancaktar[a]; Aydin Turgut[b]; Fei Guo[c]
[a] Mechanical and Aeronautical Engineering Department, Clarkson University, Potsdam, NY, U.S.A. [b] Mechanical Engineering Department, Firat University, Elazig, TURKEY [c] Mechanical Engineering Department, Jinzhou Institute of Technology, PRC

To cite this Article Sancaktar, Erol , Turgut, Aydin and Guo, Fei(1992) 'Viscoelastic and Processing Effects on the Fiber-Matrix Interphase Strength. Part I. The Effects of Loading Rate, Test Temperature, Fiber Sizing and Global Strain Level', The Journal of Adhesion, 38: 1, 91 — 110
To link to this Article: DOI: 10.1080/00218469208031269
URL: http://dx.doi.org/10.1080/00218469208031269

J. Adhesion, 1992, Vol. 38, pp. 91–110
Reprints available directly from the publisher
Photocopying permitted by license only

Printed in the United Kingdom

Viscoelastic and Processing Effects on the Fiber-Matrix Interphase Strength. Part I. The Effects of Loading Rate, Test Temperature, Fiber Sizing and Global Strain Level*

EROL SANCAKTAR

Mechanical and Aeronautical Engineering Department, Clarkson University, Potsdam, NY 13699-5725, U.S.A.

AYDIN TURGUT

Mechanical Engineering Department, Firat University, Elazig, TURKEY

FEI GUO

Mechanical Engineering Department, Jinzhou Institute of Technology, PRC

(Received April 25, 1991; in final form January 13, 1992)

The effects of loading rate, fiber sizing, test temperature and global strain level on the adhesion strength between carbon fibers and a thermosetting epoxy (Epon 815) are studied using the single fiber fragmentation test procedure. Analytical methodology describing the viscoelastic behavior observed is also presented. The possibility of rate-temperature-interphase thickness superposition for the interfacial strength function is illustrated based on the analytical models discussed. Experimental data are discussed using Weibull statistics and also presented in the form of percent relative frequency histograms for the fiber fragments in a collective fashion. The use of histograms allows for interpretation of the skewness in the data population.

KEY WORDS Fiber-matrix interphase, single-fiber fragmentation test, fiber sizing, rate-temperature-interphase thickness superposition, nonlinear viscoelastic stress analysis, critical fiber fragment size.

INTRODUCTION

Previous work on adhesively bonded joints has clearly shown that the strength of the bond and the mode of failure (*i.e.*, cohesive *versus* adhesive) are affected by the rate of loading, environmental temperature and the surface treatment procedure for the substrates. For example, Lin and Bell[1] report that in their experiments on

*Presented in part at the 14th Annual Meeting of The Adhesion Society, Inc., Clearwater, Florida, U.S.A., February 17–20, 1991.

tubular butt specimens all joints without chemical surface treatment failed adhesively. Specimens whose adherend surfaces had been chemically treated contained cohesive and adhesive failure regions. Bond strengths for chemically-treated surfaces were always greater than for untreated surfaces.

One of the pioneering viscoelastic studies on the mechanisms of adhesive failure was published by Hata.[2] He reports that (in the absence of surface treatment effects) "variability of failure modes is essentially of rheological character, depending on rate of separation, temperature, thickness of adhesive layer, and its physical properties". Hata, however, assumes that the interfacial force is essentially elastic and its energy at failure is equal to the stored elastic energy in the bulk adhesive (layer) phase at the time of interfacial failure. With his model, Hata proposes mutual reduction between rate, temperature, and thickness, predicts transition from cohesive to interfacial failure and shows that interfacial strength increases with increasing rate. Of course, rate-temperature superposition in polymeric materials has been a known fact for several decades. For example, Bartenev and Zuyev[3] report that: "the increase of strain rate is equivalent to a lowering of temperature. A rapid fracture—at a high strain rate—is therefore equivalent to a low-temperature one, and a slow one—at a low strain rate—to a high-temperature fracture of viscoelastic materials."

Rate-time-temperature dependence of the stress-strain and failure behavior of structural adhesives in the bonded lap shear mode was shown by Sancaktar *et al.*[4,5,6,7] They fitted viscoelastic models to describe the stress-strain behavior and mathematically modeled the rate and time dependence of the failure stresses. The equation used to describe rate dependent failure was similar to Ludwik's equation[8] (*i.e.* log-log relation between stress and strain rate) but included a temperature term to allow for parallel shifts.[5,7] Similar rate dependence was later shown by Sharon *et al.*[9] except that the temperature shifts observed in the log-log behavior of stress *versus* strain rate was not parallel but of converging or diverging nature depending on the adhesive and presence of carrier.

Studies summarized above did not treat the interphase as a separate viscoelastic entity with thickness and (viscoelastic) material properties. Adequate analysis and understanding of the interphase between an adherend (fiber) and an adhesive (matrix), however, is critical for design of efficient bonded structures and composite materials. In adhesion science and technology circles it is a well accepted fact that the mechanical properties of the (polymeric) adhesive material is altered in regions close to the adherend due to the adhesion process. For example, approximately 10% reduction in the adhesive bulk shear modulus has been reported in the literature, in an interphase region comprising approximately 20% of the bulk adhesive thickness.[10] Consequently, a satisfactory mechanical analysis on the adherend-adhesive interaction should include a finite width interphase with its own material properties rather than assuming an interface with unknown properties or very high strength and negligible thickness. Modelling of the adhesive-adherend interphase becomes especially relevant in understanding and design of composite materials with "tailored" interphases which increase the toughness of the composite material. A main reason for the presence of such a region is attributed to the sizing applied to assist processing during prepreg or filament winding operations and also to improve adhesion. Obviously, diffusion of this sizing into the matrix can create a concentra-

tion gradient. There is a variety of other possible mechanisms which could lead to an interphase region. For example, possible polymeric diffusion into the fiber substrate during the adhesion process, selective adsorption of one or more of the components in the matrix before curing, and free volume differences between the bulk polymer and the polymer near the fiber-matrix boundary possibly created by thermal stresses.

In fiber-matrix bonding, which is the topic of this paper, a common method of measuring the quality of adhesion is the single-fiber-fragmentation test procedure. This procedure involves a simple composite sample coupon with a single fiber embedded in a (preferably transparent) matrix. The coupon is loaded in the tension mode globally and the load is transferred to the embedded fiber *via* the interphase which is often assumed to be under a dominant state of shear. The shear stress transferred in this fashion is equilibrated by a tensile stress on the fiber itself as required by the mechanical equilibrium condition. This tensile stress, when larger than the ultimate strength of the fiber, causes the fiber to fragment. Fiber fragmentation continues until the length of the fragment (*i.e.* fragment circumferential surface area) is not enough to transmit the interfacial shear stress as a tensile load high enough to break the fiber. The fiber length at this end point of the fragmentation process is called the critical fiber length, l_c, and is assumed to be (linearly) proportional to the interfacial shear stress based on elastic equilibrium conditions and the state of "pure" shear which is assumed to exist at the interphase.

Various elastic and elastic-plastic approaches have been used in the literature to study the micro-mechanics of stress transfer between fiber and matrix. Assuming uniform fiber strength and diameter, and using elastic-plastic analysis, Kelly[11] derived an expression for adhesion strength, τ_c, in the form

$$\tau_c = (\sigma_f \, d)/(2 \, l_c) \tag{1}$$

where:
τ_c = the shear strength at the fiber-resin interface,
d = the fiber diameter,
l_c = the critical fiber fragment size,
σ_f = the fiber tensile strength.

As described by Kelley, when a tensile load is applied to the fiber-matrix composite, the fiber should break into fragments until l_c is reached which is too short to transfer stress equal or greater than σ_f. The l_c is believed to indicate the adhesion condition. In other words, shorter l_c means larger shear stress τ_c which shows better adhesion.

Recent work by Sancaktar *et al.*,[12] however, showed that nonlinear viscoelastic behavior of the matrix and the interphase may have a profound effect on the mechanism of stress transfer.

Sancaktar's analytical model involves a cylindrical interphase surrounding an elastic fiber of finite length. The interphase region has nonlinear viscoelastic material properties. The region surrounding the interphase (which can be assumed to be the bulk of the adhesive matrix) is also assigned nonlinear viscoelastic properties which are different from those of the interphase. The nonlinear viscoelastic material behavior of the interphase zone and the matrix is represented using a stress-

enhanced creep. Different interphase diameter values and different material properties for the interphase and the matrix are used to determine their effects on the interfacial shear stress. Results of this analysis reveal that depending on the relative magnitudes of interphase and matrix viscoelastic material properties it is possible to have stress reductions or increases along the fiber and, hence, the critical fiber length obtained will also vary accordingly. This result reveals that not only the quality of adhesion but also the material properties of the bulk matrix and the interphase, all of which can be affected by cure conditions, can affect the critical fiber length which is widely used as the gauge by which fiber-matrix interfacial strength is perceived.

THEORETICAL CONSIDERATIONS

Adhesives are usually molecular high polymers. As the mechanical stress-strain properties of polymers are strongly influenced by time and temperature, and are strongly viscoelastic in certain temperature regions, then either bulk or bonded mechanical stress-strain properties of adhesives would be expected to be similarly viscoelastic.

The nature of load transfer between the substrates *via* the adhesive and the interphase is quite complex, especially when any of the constituents exhibit viscoelastic behavior. For example, Sancaktar *et al.* showed that[13] when aluminum adherends are bonded with Metlbond 1113 (Narmco) modified epoxy adhesive (with carrier cloth) in a symmetrical single lap geometry, the joint can exhibit relaxation and creep behaviors simultaneously depending on the location of measurement. Figure 1 illustrates this behavior: When constant strain is maintained at the ends of aluminum adherends the joint relaxes while the elastic recovery of the adherends exerts tensile forces on the adhesive which strains as shown in Figure 1. Obviously, considerable strain transfer occurs between the two materials, causing the adhesive to creep under fixed displacement boundary conditions for the adherends.

In order to describe the rate dependence of limit stress and elastic limit strain for polymeric and adhesive materials in the bulk form, Brinson *et al.*[8,13] utilized a semiempirical approach proposed by Ludwik (reported by Thorkildsen) in the form:

$$\tau_{ult} = \tau' + \tau'' \log(\dot{\gamma}/\dot{\gamma}') \tag{2}$$

where:

τ_{ult} = ultimate shear stress,
$\dot{\gamma}$ = initial elastic strain rate, and
τ', τ'', and $\dot{\gamma}'$ = material constants.

Brinson *et al.*[8,13] used the same form of equation (2) to describe the variation of elastic limit shear stress (τ_{el}) and strains (ϕ) with initial elastic strain rates. These expressions may be written as:

$$\tau_{el} = \theta' + \theta'' \log(\dot{\gamma}/\dot{\gamma}') \tag{3}$$

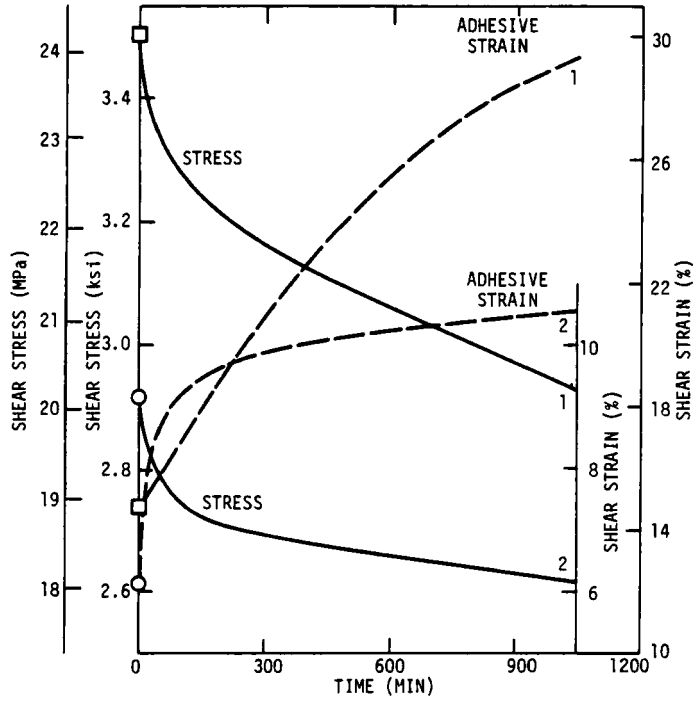

FIGURE 1 Adhesive Relaxation Behavior of Two Metlbond 1113 Symmetric Single Lap Specimens (Constant Deformation was Maintained at the End of Adherends).

and,

$$\phi = \phi' + \phi'' \log(\dot{\gamma}/\dot{\gamma}') \tag{4}$$

where additional material constants are defined accordingly. Sancaktar *et al.* later showed applicability of equations (2) through (4) for adhesives in the bonded form and also proposed superposition of temperature effects on these equations.[5,7]

The theoretical basis of equation (2) can be found in the Eyring Theorem according to which the mechanical response of an adhesive is a process that has to overcome a potential barrier, (ΔE). We think that this barrier decreases not only with increasing stress but also with increasing temperature. Based on the Eyring Theorem the relationship between a limit stress, say τ_{el}, and the strain rate can be written as:

$$\dot{\gamma} = A \exp[(\tau_{el} V - \Delta E)/RT] \tag{5}$$

where:
A = a pre-exponential factor,
R = the gas constant, and
V = the activation volume.

Equation (5) can be expressed in logarithmic form as:

$$\tau_{el} = \Delta E/V + [2.303RT \log(\dot{\gamma}/A)]/V. \tag{6}$$

Sharon *et al.*[9] recently applied equation (6) to describe rate and temperature dependent variation of four structural adhesives in the bulk form. They used the shift factor $[\log(1/A)] \times 10^{-3}$ on the temperature (°C) to describe the effect of rate.

If the energy barrier term $\Delta E/V$ of equation (6) is also affected by temperature then one needs two shift factors in equations (2) through (4) to describe rate-temperature effects on limit stress-strain equations:

$$\tau_{el} = \{a_{T1}\}\ \theta' + \{a_{T2}\}\ \theta''\ \log(\dot{\gamma}/\dot{\gamma}') \tag{7}$$

and,

$$\phi = \{b_{T1}\}\ \phi' + \{b_{T2}\}\ \phi''\ \log(\dot{\gamma}/\dot{\gamma}') \tag{8}$$

where:
a_{Ti}, b_{Ti} = shift factors as functions of temperature.

In order to analyze the effects of rate and temperature on the interfacial strength (as measured by fiber fragment length) one can initially use a simple energy approach in the following manner: A critical energy level, W_c, is used to represent interfacial failure. In the presence of matrix, fiber and interphase (which transmits the matrix energy to the rigid fiber) the combined elastic energy can be written as:

$$V_m\{(1/2)\epsilon^2_{matrix} E_{matrix}\} + V_{ip}\{(1/2)\gamma^2_{interphase} G_{interphase}\} + V_f\{(1/2)\epsilon^2_{fiber} E_{fiber}\} = W_c. \tag{9}$$

Where V_m, V_{ip} and V_f represent volume fractions of the matrix, interphase, and the fiber, respectively. Now, if one considers equation (9) in conjunction with equation (8) to include rate-temperature effects, then it can be easily deduced that higher W_c levels are obtained at high rate and/or low temperature levels since the proportion of elastic strains increases with increasing elastic limit strains due to high rate and/or low temperature levels.

Nonlinear Viscoelastic Stress Analysis of the Interphase

Recent nonlinear viscoelastic stress analysis of the fiber/matrix interphase by Sancaktar *et al.* concurs with this simplified finding.[12] In this analysis, the nonlinear viscoelastic material behavior of the interphase zone and the matrix is represented using a stress-enhanced creep. For this purpose the "power-law" creep compliance function,

$$D(t,\sigma) = D_0 + D_1(t/e^{-\theta\sigma})^n \tag{10}$$

is used. In equation (10) D_0 is the instantaneous compliance and D_1 (transient creep compliance), n (power factor for time) and θ (strength of stress contribution in time shift) are material parameters which represent the nonlinear and time dependent material behavior. Note that equation (10) incorporates a "reduced time" (t/a_σ) where the time reduction is accomplished by a stress-dependent shift factor,

$$a_\sigma = \exp(-\theta\sigma). \tag{11}$$

In order to determine the time-dependent variation of the interfacial shear stresses based on the (different) nonlinear creep compliances assigned to the fiber-matrix interphase and to the matrix, the following quasi-elastic method is used.

The interphase is assumed to be devoid of all stresses except the interfacial shear stress which is assumed to be constant throughout the thickness, δ, of the interphase. These assumptions allow the use of elastic equilibrium equations and their derivatives with respect to the axial space variable, x, (Figure 2) along with the necessary boundary conditions in obtaining time dependent interfacial shear stress values. Subsequent use of nonlinear viscoelastic material properties for the matrix does not affect the validity of this quasi-elastic solution procedure, since matrix creep strains are equated to mid-fiber elastic strains in a quasi-static fashion during the numerical

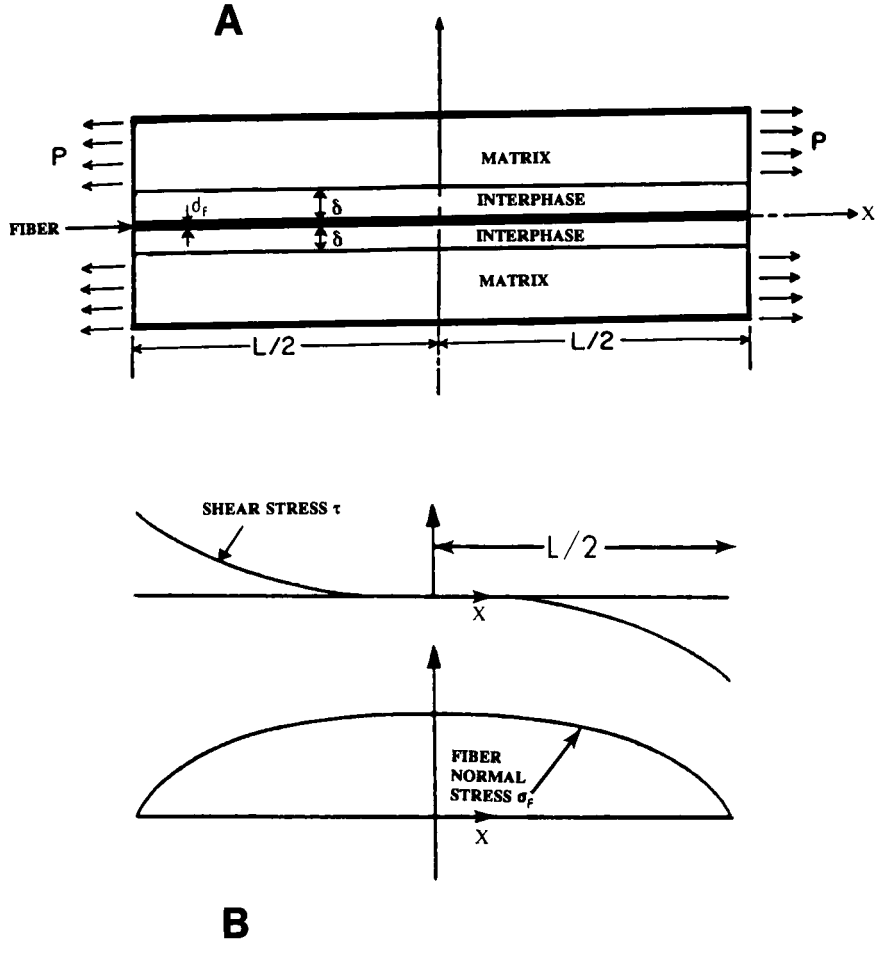

FIGURE 2 Single Fiber Composite Element Geometry (A) and the Fiber Stresses (B).

iteration procedure for the solution. This treatment renders the effect of the creep process in the matrix equivalent to increased loading of the elastic fiber. The global load level, P, of course, is assumed to be independent of the axial space variable, x, which allows the assumption $dP/dx = 0$. In order to obtain the governing state-of-stress equation, the shear strain $\gamma(t,x)$ and the shear stress $\tau(t,x)$ at the interphase of thickness δ are assumed to be produced by the difference in displacements $U_m(t,x)$ and $U_f(t,x)$ of the matrix and fiber, respectively. This assumption amounts to the application of the classical shear lag method. Subsequent to substitution and differentiation, the creep compliance equation,

$$\gamma(t) = \tau D(t) \tag{12}$$

of linear viscoelasticity is applied to our nonlinear viscoelastic case to be used in iterative solution of the resulting second order, nonlinear partial differential equation

$$[(A_f/A_m E_m) + (1/E_f)](4/\delta d_f)\ \tau(t,x) = [d^2\gamma(\tau)/d\tau^2][d\tau(t,x)/dx)]^2 + [d\gamma(\tau)/d\tau][d^2\tau(t,x)/dx^2] \tag{13}$$

where $\gamma(\tau)$ is defined by equations (10) and (12).

Boundary Conditions Due to the symmetry of the problem, we have, $\tau = 0$ at $x = 0$, and, $\tau = \tau_{max}$ at $x = L/2$, where L is the fiber length. Consequently, $\sigma_f = \sigma_{ftmax}$ at $x = 0$. Also, due to the very small cross-sectional area of the fiber ($\sim 3.85 \times 10^{-5}$ mm^2) we assume, $\sigma_f(t,x) = d\sigma_f(t,x)/dx = 0$ at $x = L/2$. This condition, along with the condition $\tau = \tau_{max}$ at that location, usually results in plastic deformation or cracking and voiding of the matrix at fiber ends. Of course, the equilibrium conditions must also be simultaneously satisfied along with these conditions.

The Iterative Solution The iterative method used to solve equation (13) is similar to the method used by Weitsman.[14] The first step in this method is successive differentiation of equation (13) with respect to the space variable, x. The availability of first through fifth space derivatives of $\tau(t,x)$ is assumed to provide sufficient accuracy for the numerical method. The next step involves expressing τ_i and $d\tau_i/dx$ by Taylor expansions with five terms assumed to provide sufficient accuracy.

The half-fiber length $0 \leq x \leq (L/2)$ is divided into N equal sub-intervals of length $\Delta = L/2N$ with $N = 500$. For iteration purposes, each space iteration node is identified as $x_i = i\Delta$ ($i = 1,2,\ldots,N$) and the corresponding shear stress to be calculated as $\tau(t,x_i) = \tau_i$.

The iteration process starts with initial guess values for τ_0' to be substituted along with the initial guess for the boundary condition, $\tau(o) = \tau_o^{(1)}$ into equation (13) to compute τ_o''. τ_o''', τ_o^{iv} and τ_o^{v} are then calculated using the derivatives of equation (13). These computed values can now be substituted into the Taylor expansions to calculate τ_1 and τ_1'. In this fashion, the iteration scheme proceeds forward until τ_N and τ_N' values are obtained.

Accuracy of the calculated τ_i values is checked by using the equilibrium condition:

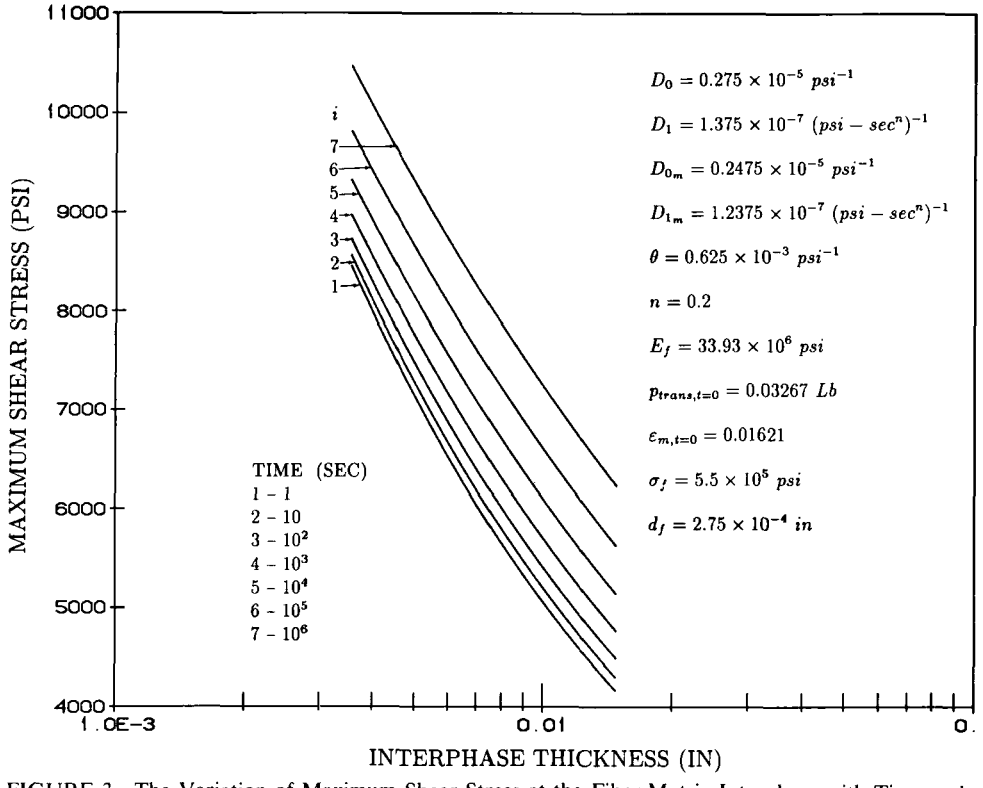

FIGURE 3 The Variation of Maximum Shear Stress at the Fiber-Matrix Interphase with Time and Interphase Thickness for Maximum Transferred Load. The Cylindrical Interphase and Matrix are Assumed to be Nonlinear Viscoelastic.

$$[d\tau(t,x)/dx]_j - (P/A_m E_m \delta)\,[d\gamma(\tau)/d\tau]^{-1} = g_j \quad \text{at} \quad x = L/2. \tag{14}$$

The necessary material and geometrical parameters used in the iteration procedure are shown in Figures 3 and 5.[12]

Results of this analysis revealed that the magnitude of rate/temperature effects on interfacial strength should depend on the thickness of the interphase and the relative magnitudes of interphase and matrix viscoelastic material properties. For example, Figure 3 shows that the fiber maximum shear stress which exists very close to the fiber ends increases with decreasing interphase thickness, while it is shown to decrease with decreasing time exposure to external loading. Note that the existence of such high stress concentrations at fiber ends usually results in interphase/matrix plastic deformation and/or cracking (Figure 4) at those locations which result in redistribution of stresses and, possibly, in lower values of average shear stresses along the fiber. Such cases are not likely to make optimum use of fiber support since the major portion of the stress distribution is concentrated very close to the fiber ends and the rest of the interphase carries little shear load. This effect of fiber end shear stress concentration on the overall distribution of the interphase shear stresses can be seen clearly in Figure 5 which was obtained for the case of a nonlinear vis-

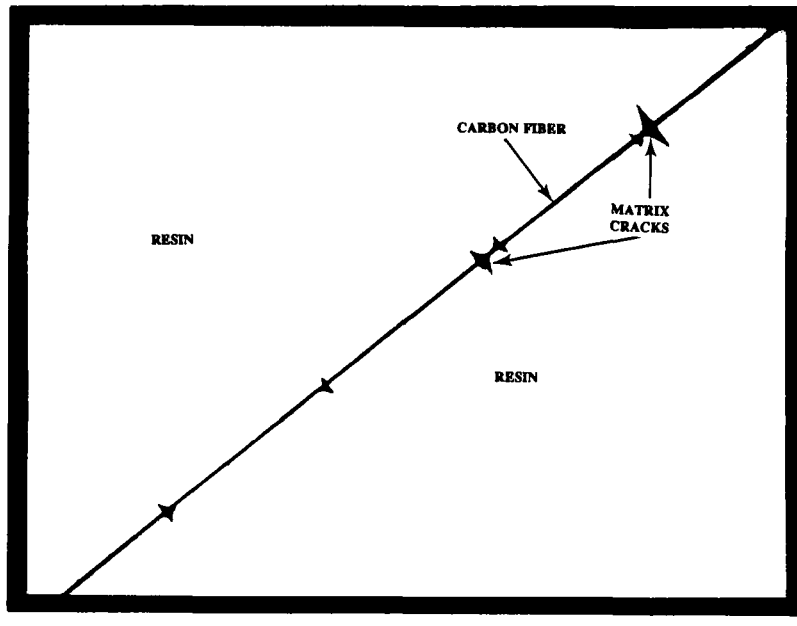

FIGURE 4 Matrix Cracks Formed as a Result of Fragmentation of a 7 μm Diameter Carbon Fiber Embedded in EPON 815 Thermoset Resin. Global Load Applied to the Single Fiber Tension Test Coupon was Transferred to the Fiber *via* Interfacial Shear Stress.

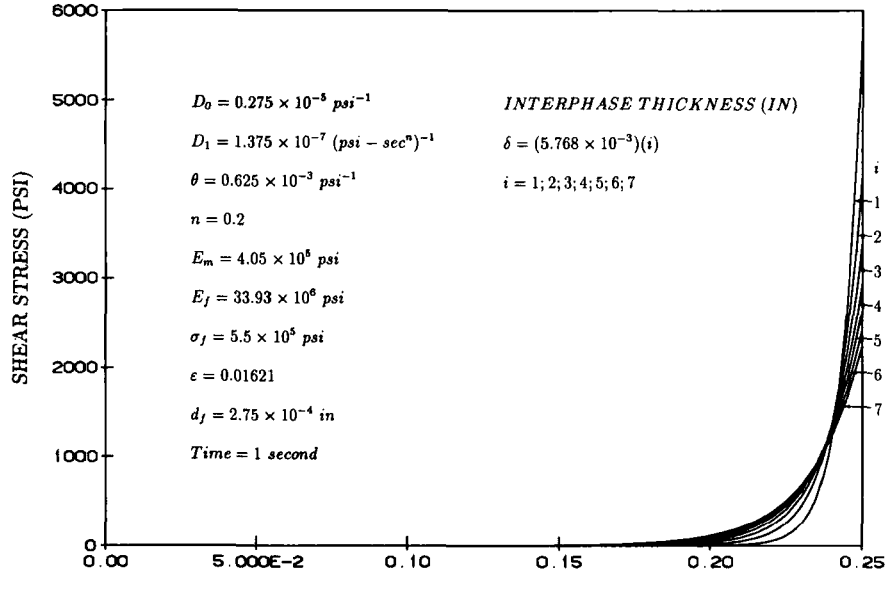

FIGURE 5 The Effect of Interphase Thickness on the Distribution of the Shear Stress at the Fiber-Matrix Interphase Based on Nonlinear Viscoelastic Analysis of a Cylindrical Interphase Zone for Time = 1 second. The Matrix is Assumed to be Linear Elastic. The Horizontal Axis Represent Distance, X (see Fig. 2) Along the Fiber Length Starting at Mid-Fiber.

coelastic interphase and linear elastic matrix material properties for demonstration purposes. Consequently, shear stresses more uniformly distributed along the fiber with smaller peaks at the fiber ends make more efficient use of the fiber support and are thought to result in shorter fragment lengths during a single fiber tension test.

Evidence from our current experiments indicates that energy-controlled fracture processes may dominate the fiber fragmentation process. This comment is made on the basis of our observations of shorter fragment lengths resulting from higher cross-head rate experiments. In such cases, the total elastic energy available from the composite system may indeed be the controlling factor for the fragment lengths obtained as indicated by equation (9). Therefore, (slower) processes involving viscoelastic dissipation over longer periods of time would be expected to result in longer fragments.

EXPERIMENTAL PROCEDURES

Single carbon fiber/epoxy resin dogbone shaped specimens were made from epoxy resin. The epoxy resin used was Shell Epon 815® (Shell Chemical), an epichlorohydrin/bisphenol A-type epoxy resin containing a reactive diluent. The curing agents were DETA (Diethylenetriamine) and Armocure 100 (Akzo Chemicals). DETA is a liquid polyamine widely used with epoxy resins for fast cures and room temperature cures, providing good resin properties at room temperature (or below 82°C, the minimum heat distortion temperature reported by the manufacturer). Armocure 100 is an aliphatic polyamine providing tough, flexible, water-resistant and solvent-resistant cured epoxy resin. 12 phr of Armocure 100 was added to the matrix composition to increase its flexibility. The composition of the epoxy matrix was 88 phr of Epon 815, 12 phr of DETA and 12 phr of Armocure 100. The cure condition was 38°C applied for 12 hours in a convection oven. The cross-head rate, environmental temperature, global strain level, and fiber surface finish were test parameters and will be indicated in each figure depicting the results. For experimentation the cross-head rate was varied between 3.18 mm/min and 254 mm/min. The test temperatures used were 54.4°C and 65.6°C, and the global strain levels used were 4% and 12%.

The carbon fiber chosen was 7μm diameter Celion G30 500 (BASF) unsized or finished with EP03 depending on the test conditions. EP03 is an epoxy sizing agent deposited through use of an emulsion. The fiber was fixed in an aluminum mold machined specifically to form single fiber tensile specimens. Care was exercised to prevent contamination of the fibers during this process. After the resin was poured into the molds, vacuum devices were used to remove air from the molded resin. The molds were then put in a convection oven for curing. After curing, the specimens were removed from the molds and machined to the required shape.

The tensile test machine for the fragmentation tests was a Model 1000 Instron Universal Testing Instrument. Strains were measured using a 4300 Plastics Testing Extensometer with a LVDT Controller. A 7000A/7001A X-Y Recorder was used to plot the stress-strain curves.

A test temperature of 54°C was used to ensure sufficient material deformability

to reach 4% strain. The use of this elevated temperature prevented brittle failures and resulted in consistent critical fiber length l_c values.

The total number of specimens used was 22, resulting in a total of (approximately) 1639 fiber fragments providing information on the four test parameters: rate, temperature, fiber sizing, and strain level. The large number of fragments is obtained due to the use of 140 mm-long specimens with 50 mm gage lengths (see Figure 3 in Part III of this series of papers). We think that a gage length fifty to one hundred times larger than the length of fiber fragments obtained is more representative of real-life, long fiber composites.

RESULTS AND DISCUSSION

For ease of interpretation and comparison the fiber fragment data are tabulated in the form of histograms. These histograms represent the percent relative frequency of occurrence for each 20×10^{-2} mm fragment length by a rectangular bar, the area of which is proportional to the frequency. Obviously, one can fit a smooth curve over a histogram which is composed of a collection of rectangular bars of equal width and varying heights. When such a curve has just one peak it is called unimodal, and if it has two peaks it is called bimodal. The part of the curve away from the peak on either side is called a tail. When the two tails of a distribution are identical it is called symmetrical. If one of the tails is longer than the other, it is called skewed. When the long tail extends out to the left, the curve is negatively skewed and if it extends out to the right it is positively skewed. The important consideration for a skewed distribution is that the mean, $X' = \Sigma X_i/N$, is further out toward the long tail than the median. In other words, the mean (*i.e.* the average fiber fragment length in our calculations) is more influenced by the extreme values. In our case, the median describes the length of a typical fiber fragment while the mean describes the typical fragment length, *i.e.* the average fiber fragment length.

We believe that in interpreting the fragment histograms it is necessary to pay attention to the type of skewness and, consequently, the relative positions of the mean, which is tabulated on each histogram, and the median which can be visually interpreted. We think that in a fragmentation test the physical effects resulting in a negative skew in data (*i.e.* the long tail consisting of short fragments) would be different from those that would result in a positive skew (*i.e.* the long tail consisting of long fragments). The causes of negative skew may be: i) presence of gas bubbles or other inclusions at the interphase region resulting in stress concentration, ii) crosslinking gradients in the interphase and/or matrix along the fiber, iii) residual stresses, iv) other stress concentrations, v) a low strength (defective) length of carbon fiber. During our experiments the effect i) mentioned above was excluded, since all specimens were visually inspected under a microscope. We think that effects ii) and iii) are unlikely for our specimens, since the resin mixtures were thoroughly mixed and the cured samples were conditioned and tested at 54°C environmental temperature.

The presence of a positive skew, on the other hand, can be attributed to waviness or off-center eccentricity of the embedded fiber, and localized deformation concen-

trations and/or crack initiation and propagation in the matrix where fiber fragmentations have taken place. In such cases, deformations are not transmitted to all of the fibers to fragment them further. Consequently, a positive skew may not give a true indication of the interfacial strength. Based on these arguments we can conclude that while a negative skew may provide a true gauge of interfacial strength, it is likely that a positive skew would not.

Based on the skewness considerations explained above, it was decided that comparison and interpretation of the fragment frequency histograms would be more efficient if they were plotted collectively on the same chart for common cure conditions or curing agent content. Such graphs are shown in Figures 6 through 11. The reader should note that in all of the histograms the test conditions which result in the lowest average (mean) fragment length values result in the highest frequency bars, corresponding to shorter fragments on the left hand side of the diagrams, irrespective of their standard deviation values.

Figure 6 shows that the level of global strain above 4% does not affect the average fiber fragment length significantly. We should also note that the ultimate elongation for the carbon fiber is 1.62% (1.39% minimum) as reported by the manufacturer. Consequently, the data to be presented below studying the effects of test rate, temperature and fiber sizing were obtained at 4% global strain level.

The effect of cross-head rate on fiber matrix adhesion is shown in Figures 7 and 8 for unsized and sized fibers, respectively. Both figures reveal, clearly, that fiber fragment length is smaller at higher cross-head rates. Consequently, the interfacial

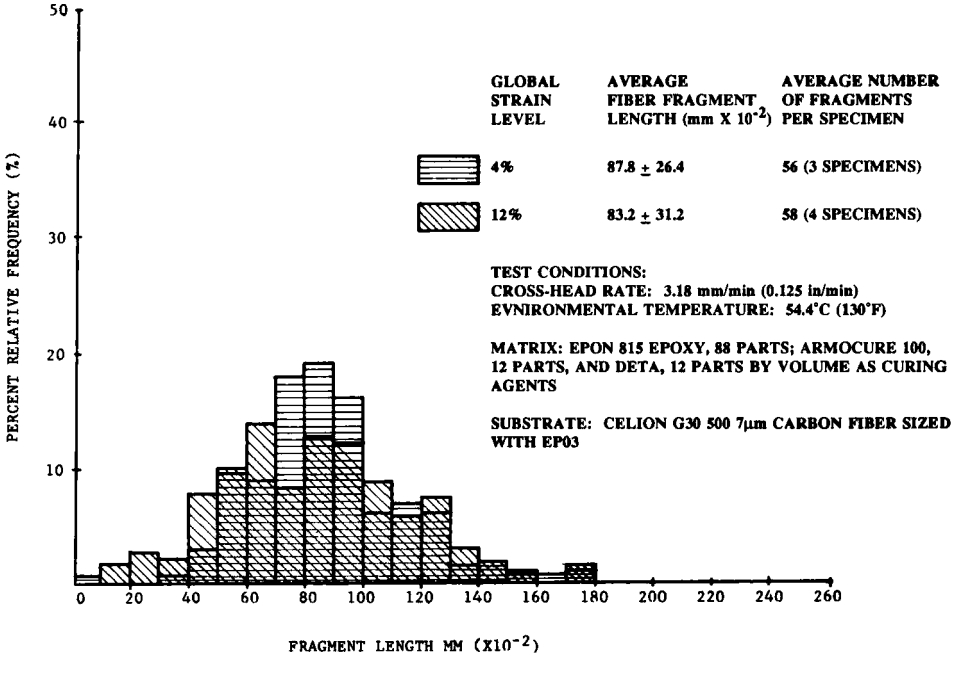

FIGURE 6 The Effect of Global Strain Level on Fiber-Matrix Adhesion as Indicated by Fragment Size Distribution in Single Fiber Tension Test Specimens with Sized Fibers.

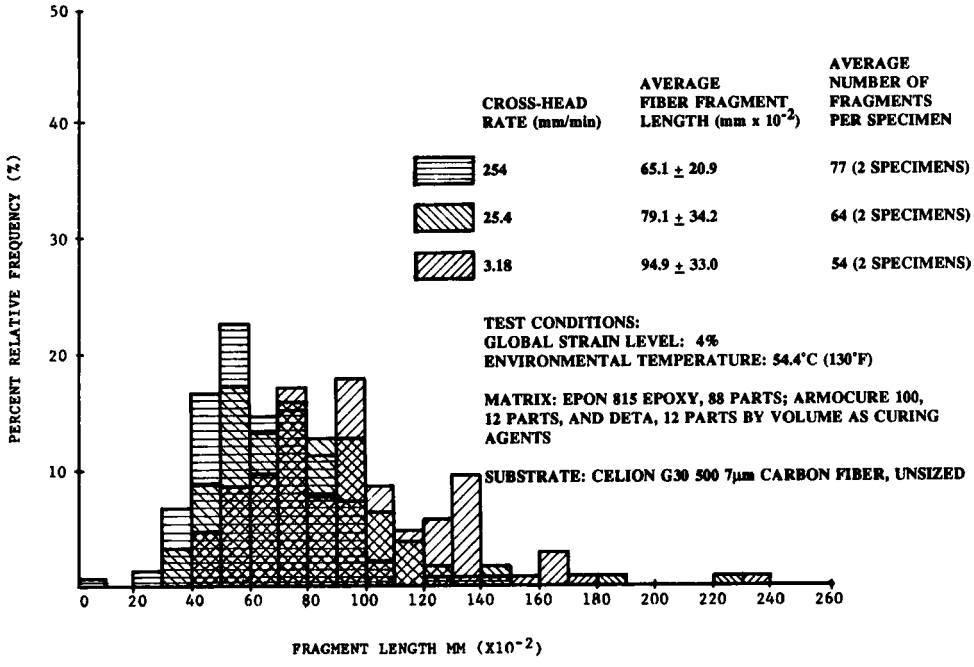

FIGURE 7 The Effect of Cross-Head Rate on Fiber-Matrix Adhesion as Indicated by Fragment Size Distribution in Single Fiber Tension Test Specimens with Unsized Fibers.

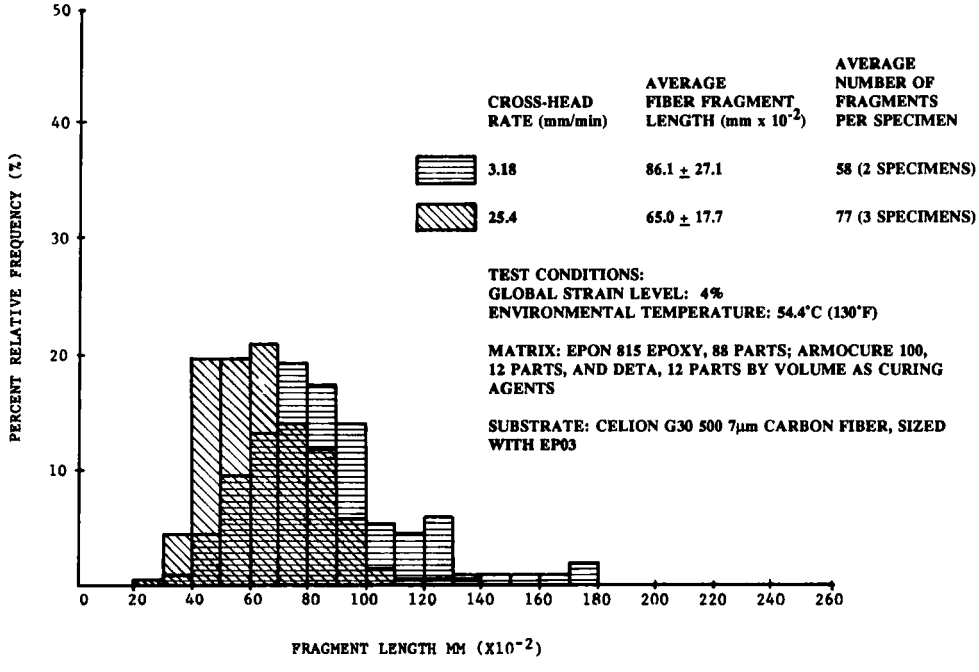

FIGURE 8 The Effect of Cross-Head Rate on Fiber-Matrix Adhesion as Indicated by Fragment Size Distribution in Single Fiber Tension Test Specimens with Sized Fibers.

strength is interpreted to be higher at higher strain (loading) rates. It should also be noted that the fragment lengths obtained are shorter for sized fibers in comparison with unsized fibers at comparable cross-head rates (Figure 8). This difference, however, is not constant but becomes larger at higher rates. This effect is illustrated clearly by comparing Figures 9 and 10 which show combined fragment frequency histograms for sized and unsized fibers tested at 25.4 mm/min and 3.18 mm/min cross-head rates, respectively.

In the Introduction section we stated that for polymeric materials the increase of strain rate is equivalent to a lowering of temperature. So far, we have shown that increases in strain rate result in shorter fiber fragment lengths. The applicability of rate-temperature superposition, as stated, on the fragment length and, consequently, on interfacial strength, is demonstrated with Figure 11. This figure shows that reductions in the environmental temperature result in shorter fragment lengths. Obviously, the effect of environmental temperature in the 66 to 54°C range is rather strong for our specimens, since reduction in average fragment length is more than twofold.

In order to confirm our conclusions discussed above, based on the data presented, additional statistical analyses were performed using a commercially-available SAS computer program. The data were fitted to a Weibull distribution, assuming a constant origin of 0, and comparing the shape (β) and location (η) parameters. This method has several advantages over comparing the simple descriptive statistics.

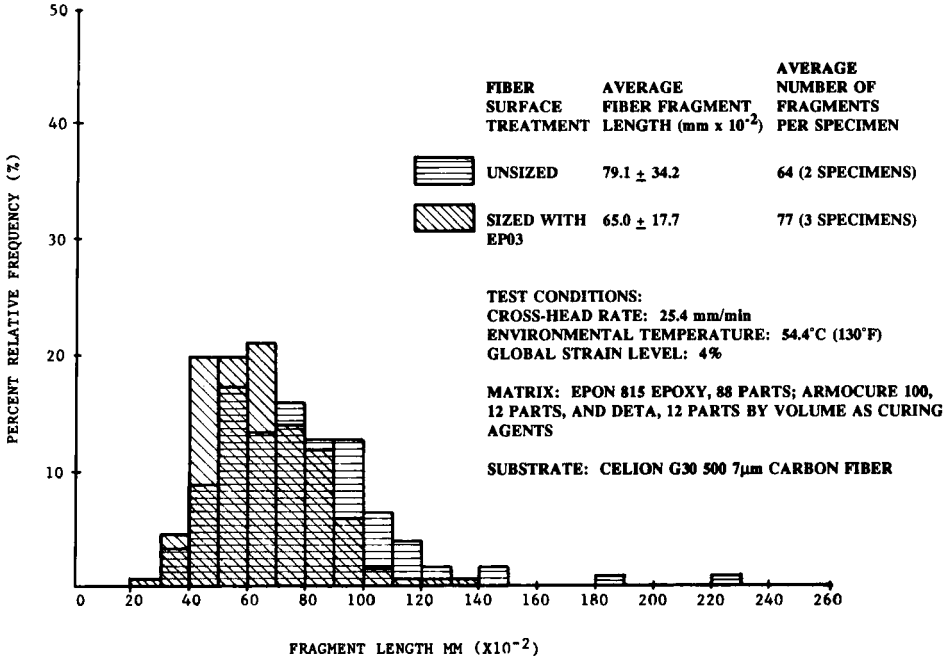

FIGURE 9 The Effect of Fiber Surface Treatment on Fiber-Matrix Adhesion as Indicated by Fragment Size Distribution in Single Fiber Tension Test Specimens Tested Using 25.4 mm/min Cross-Head Rate.

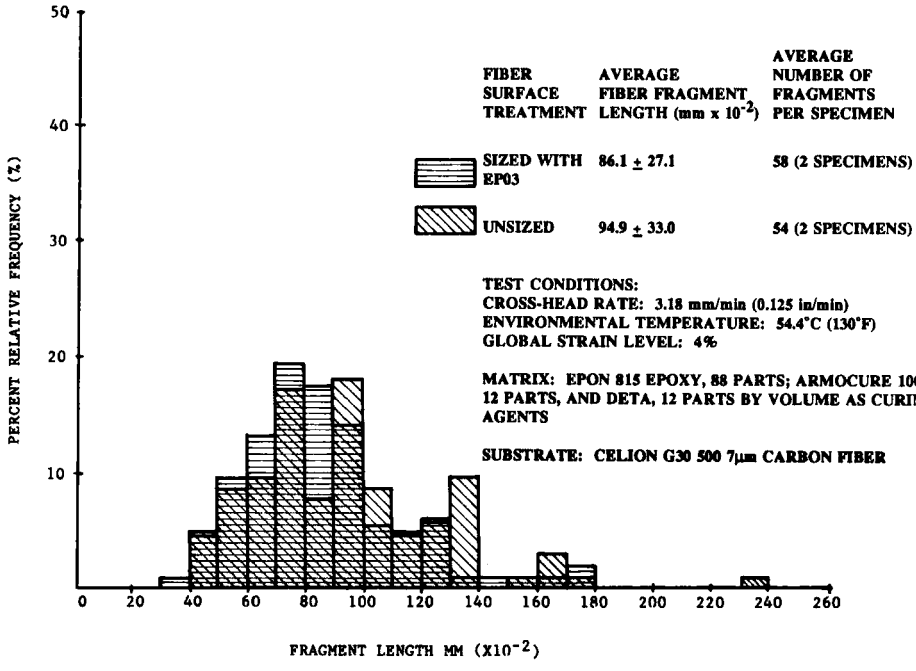

FIGURE 10 The Effects of Fiber Surface Treatment on Fiber-Matrix Adhesion as Indicated by Fragment Size Distribution in Single Fiber Tension Test Specimens Tested Using 3.18 mm/min Cross-Head Rate.

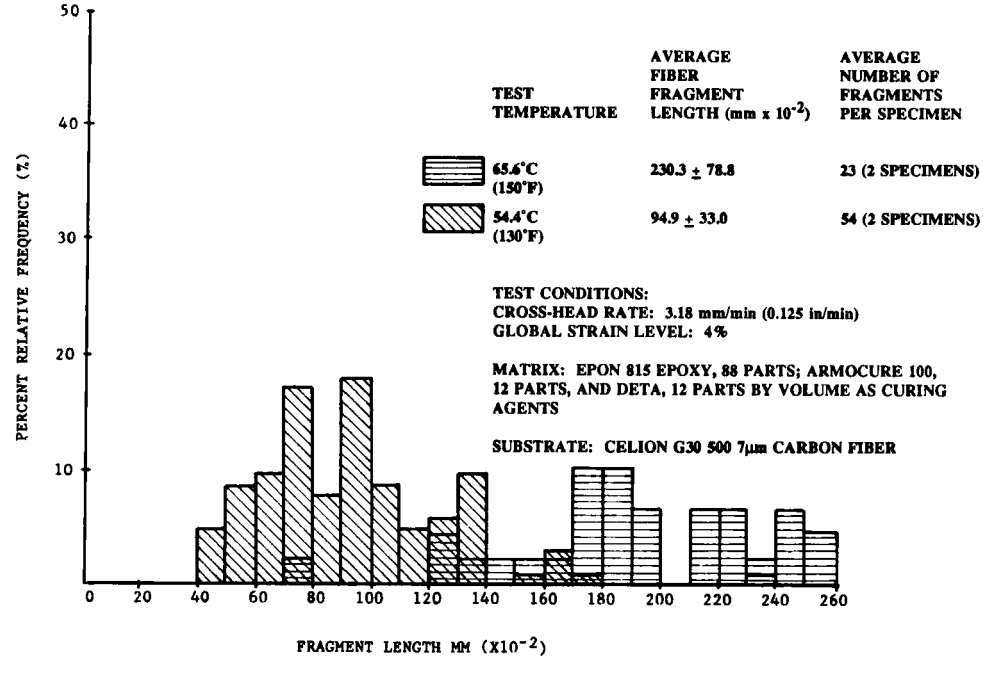

FIGURE 11 The Effect of Test Temperature on Fiber-Matrix Adhesion as Indicated by Fragment Size Distribution in Single Fiber Tension Test Specimens with Unsized Fibers.

First, the shape parameter gives an indication of the shape of the data, which can range from exponential ($\beta = 1.0$) to peaked normal ($\beta = 5.0$), as shown in Figure 12. This parameter can, therefore, be used to assess the influence of contributors to fiber fragmentation other than the test parameters applied. These parameters were discussed at the beginning of this Results and Discussion section. Note that when such influence is strong the parameter β approaches the value one, and the standard deviation value for the corresponding data is expected to be high. Consequently, variations in the standard deviation provide additional insight into the data obtained and such data need not be dismissed as uninformative. Especially with the single fragmentation test, use of longer gage lengths, as in this work, increases the likelihood of obtaining high and varying standard deviations. We note, however, that in this case longer gage length specimens are better representative of real-life, long fiber composites.

The location parameter, η, of the Weibull distribution always marks the location of 63.2% of the data, regardless of the shape. This parameter can be used to assess the characteristic value for the condition (*i.e.* test parameter) and compare it with others.

Figure 13 shows the variations in the Weibull shape parameter for fragment length as obtained using different cure conditions (experimental details are provided in Part II of this series of papers). Obviously, the cure conditions applied in this Part I (*i.e.* cure at 38°C for 12 hours with 12 phr DETA) provide closest to peaked normal data distribution. Other cure conditions result in data distribution varying between exponential to log normal ($\beta = 2.5$) and need to be analyzed using the biased histogram method introduced in this paper (see Part II of this series of papers).

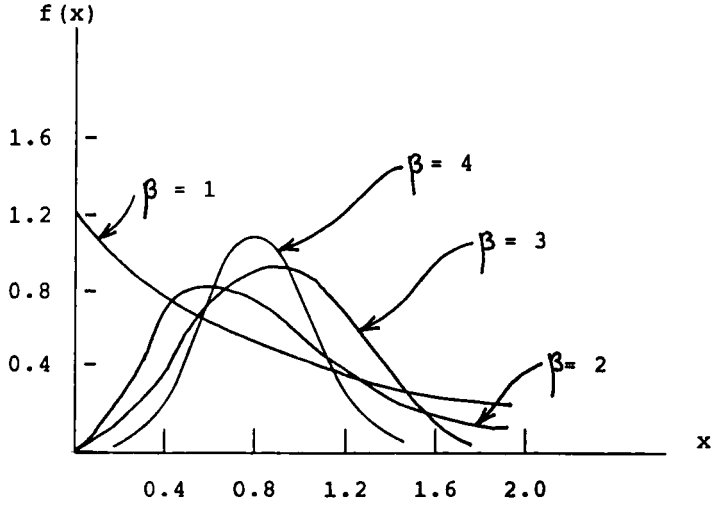

FIGURE 12 Weibull Distributions with Different Shape Parameters, β.

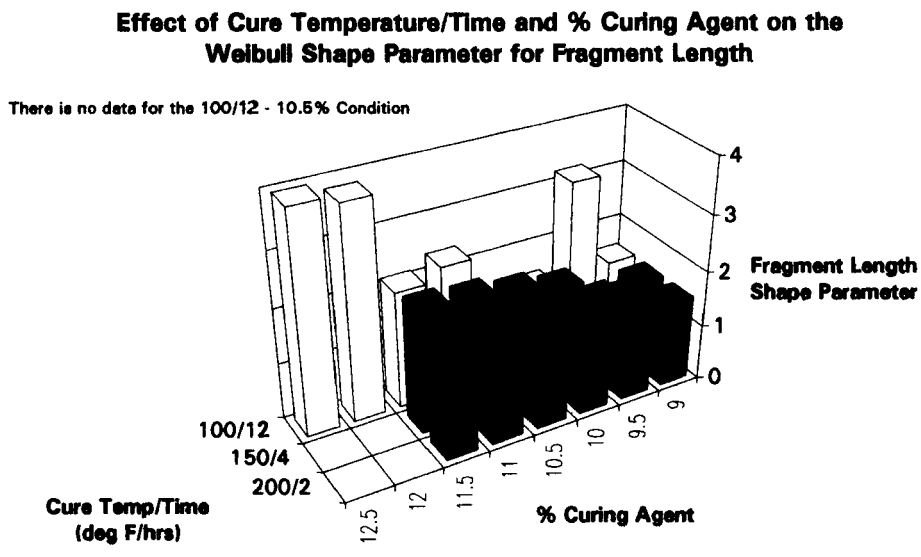

FIGURE 13 The Effect of Cure Temperature/Time and Percent Curing Agent on the Weibull Shape Parameter, β, for Fiber Fragment Length.

Figure 14 shows the variation in Weibull shape parameter for fragment length as obtained using different cross-head rate, fiber sizing, test temperature, and global strain levels. Data distributions vary between log normal and normal ($\beta = 3.44$). Reductions in β values are noted with increasing strain level and also in the absence of sizing.

Figure 15 shows the variation in Weibull location parameter for fragment length as obtained using different cross-head rate, fiber sizing and global strain levels. These variations confirm our earlier conclusions for these test parameters. In other words, the perceived interfacial strength based on the critical fiber length obtained is higher with sizing and, especially, at higher cross-head rates.

The analytical and experimental results presented so far reveal the possibility for mutual reduction between rate, temperature, and interphase thickness. If we assume that application of fiber sizing results in thicker interphases and that the cross-head rate, v, can be related to the shear strain rate, $\dot{\gamma}$, and the interphase thickness, δ, with the relation:

$$v = f(\dot{\gamma})\ g(\delta) \tag{15}$$

based on classic shear lag analysis (also based on definition of shear strain), we can then argue that for a fixed strain rate (function) the effect of increased cross-head rate can be induced by increasing the interphase thickness (*i.e.* by application of fiber sizing). For example, in the simple case of constant strain rate loading we have:

$$\gamma = \dot{\gamma} t = \Delta L/\delta. \tag{16}$$

Note that the definition of shear strain has been used on the right hand side of equation (16). Consequently, we can write:

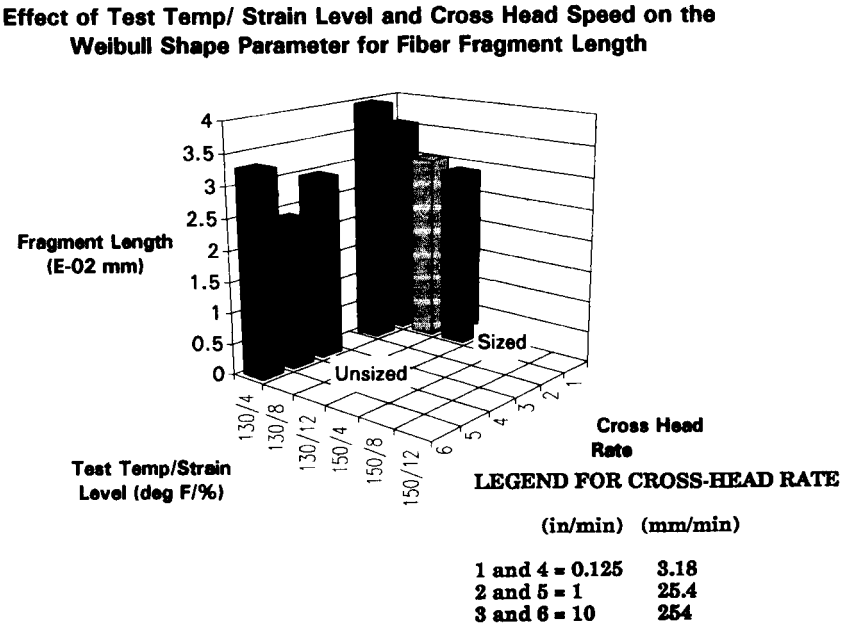

FIGURE 14 The Effect of Test Temperature/Strain Level and Cross-Head Speed on the Weibull Shape Parameter, β, for Fiber Fragment Length.

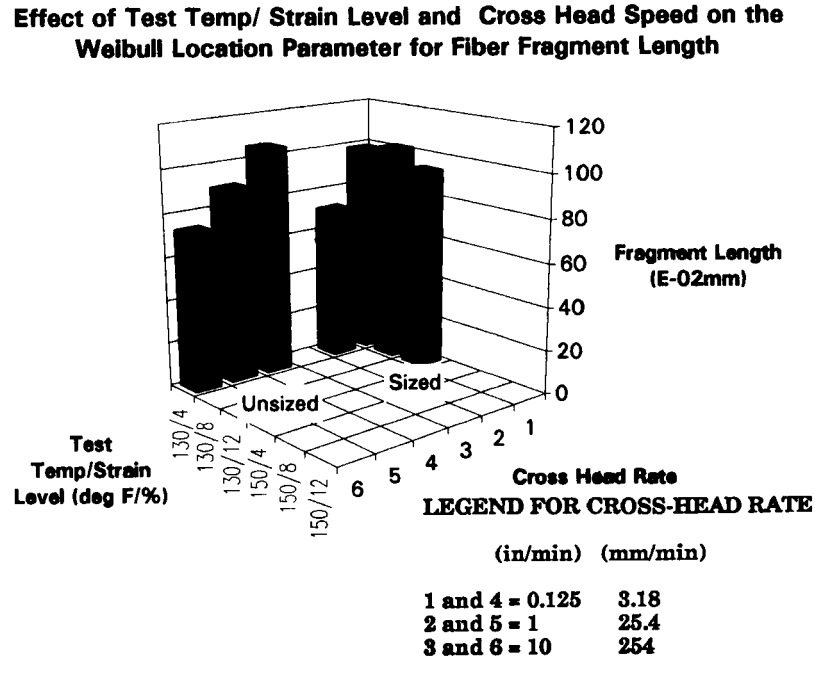

FIGURE 15 The Effect of Test Temperature/Strain Level and Cross-Head Speed on the Weibull Location Parameter for Fiber Fragment Length.

$$\Delta L/t = v = \gamma\delta/t = \dot{\gamma}\delta. \tag{17}$$

Indeed, the experimental results reveal shorter fragment length for increased cross-head rate and/or presence of fiber sizing. Based on this premise we can write the following superposition relation for the interfacial strength:

$$\tau_c = \tau_c(T_o, a_v v, a_\delta \delta). \tag{18}$$

CONCLUSIONS

The single fiber fragmentation test procedure was used to study the effects of global strain level, cross-head rate, environmental temperature and fiber sizing on the interfacial strength between carbon fibers and cured Epon 815 epoxy. The experimental results showed that the average value of the fiber fragment length is not affected significantly above 4% global strain level. Fiber sizing results in shorter fragment lengths. Increases in strain rate and reductions in environmental temperature both result in shorter fragment lengths. The effects of strain rate and environmental temperature were predicted using analytical models which were confirmed by experimental results. The data obtained demonstrated the possibility of rate-temperature-interphase thickness superposition for the interfacial strength function.

Acknowledgements

This work was performed during sabbatical visits by Mr. Fei Guo (Sept. 1987 to Nov. 1988) and Dr. Aydin Turgut (April 1989 to mid-Feb. 1990) at Clarkson University. We express our thanks to Firat University, Elazig, Turkey (Dr. Turgut) and Jinzhou Institute of Technology, People's Republic of China (Mr. Guo) for providing the permission and financial support for Messrs. Turgut and Guo's sabbatical visits at Clarkson University.

Valuable help in statistical (Weibull) analysis of the data by J. I. MacCrindle of ALCOA (Massena Plant) is gratefully acknowledged.

Partial financial support by Grumman Corporation is also gratefully acknowledged.

References

1. C. J. Lin and J. P. Bell, *J. Appl. Poly. Sci.* **16,** 1721 (1972).
2. T. Hata, *Organic Coatings and Plastics Chemistry* **31,** 193 (1971).
3. G. M. Bartenev and Y. S. Zuyev, *Strength and Failure of Viscoelastic Materials* (Pergamon Press, NY, 1968).
4. E. Sancaktar and S. Padgilwar, *J. Mechanical Design* **104,** 643 (1982).
5. E. Sancaktar, S. C. Schenck and S. Padgilwar, *Ind. and Eng. Chem. Product Res. and Dev.* **23,** 426 (1984).
6. E. Sancaktar and S. C. Schenck, *Ind. and Eng. Chem. Product Res. and Dev.* **24,** 257 (1985).
7. E. Sancaktar *Int. J. Adhesion and Adhesives* **5,** 66 (1985).
8. H. F. Brinson, M. P. Renieri and C. T. Herakovich, *ASTM STP 593,* 177 (1975).
9. Sharon, G., Dodiuk, H., and Kenig, S., *J. Adhesion* **31,** 21 (1989).
10. G. C. Knollman and J. J. Hartog, *J. Adhesion* **17,** 251 (1985).
11. A. Kelly and W. R. Tyson, *Mech. Phys. Solids* **13,** 329 (1965).
12. E. Sancaktar and P. Zheng, *J. Mech. Design* **112,** 605 (1990).
13. E. Sancaktar and H. F. Brinson, *Adhesion and Adsorption of Polymers,* L. H. Lee, Ed. (Plenum Press, NY, 1980), p. 141.
14. Y. Weitsman, *J. Adhesion* **11,** 279 (1981).